



Machine learning for in-process end-point detection in robot-assisted polishing using multiple sensor monitoring

Tiziana Segreto^{1,2} · Roberto Teti^{1,2}

Received: 18 January 2019 / Accepted: 6 May 2019 / Published online: 19 May 2019
© Springer-Verlag London Ltd., part of Springer Nature 2019

Abstract

The decision on polishing operation stopping time when employing a robot-assisted polishing machine is a critical issue for the full automation of the polishing process. In this paper, a machining learning approach based on artificial neural networks was developed using multiple sensor monitoring data to realize an intelligent system capable to determine the state of the polishing process in terms of target surface roughness achievement. During the experimental tests, surface roughness measurements were performed on each polished workpiece and the acquired sensor signals were analyzed and processed by applying two kinds of feature extraction procedures: statistical features extraction and principal component analysis. By feeding diverse types of feature pattern vectors to artificial neural networks, a highly accurate classification of the polishing process state was obtained using the principal component feature pattern vectors.

Keywords Machine learning · Artificial neural networks · Robot-assisted polishing · Multiple-sensor monitoring · Principal component analysis · Sensor fusion

1 Introduction

Polishing is an abrasive process performed in multiple phases in order to finish a workpiece with the desired surface quality. For each polishing phase, a specific level of scratches is achieved using a dedicated tool until the required degree of surface roughness is obtained. Decision making on the exact time to move to the next polishing phase, where a different tool with finer abrasive grit size needs to be used, is a critical issue. As a matter of fact, if the running polishing phase continues for too long, the occurrence of over-polishing can result in leaving undesired marks on the workpiece surface. On the other hand, if the tool is changed too early, the current phase cannot adequately remove the scratches left on the polished surface in the preceding phase [1]. Generally, the tool needs to be changed when a steady state is reached during the polishing

process and the additional material removal no longer improves the surface roughness. In this case, the curve of the surface roughness versus time/number of passes becomes flat and its slope approaches zero [2].

In current industrial practice, a polishing process requires an expert operator to manually polish the workpiece, which makes the process laborious and time-consuming. Recently, a new type of polishing station, employing a robotic arm, has been proposed for process automation: robot-assisted polishing [3].

To ensure a fully automated polishing job, it is necessary to build a predictive system that can monitor in real time the state of the polishing process in order to reach the surface quality target, reduce the unnecessary polishing steps and increase the level of safety. A reliable in-process polish monitoring system can transform the manufacturing environment from manually operated production machines to unsupervised robotic material removal operations [4].

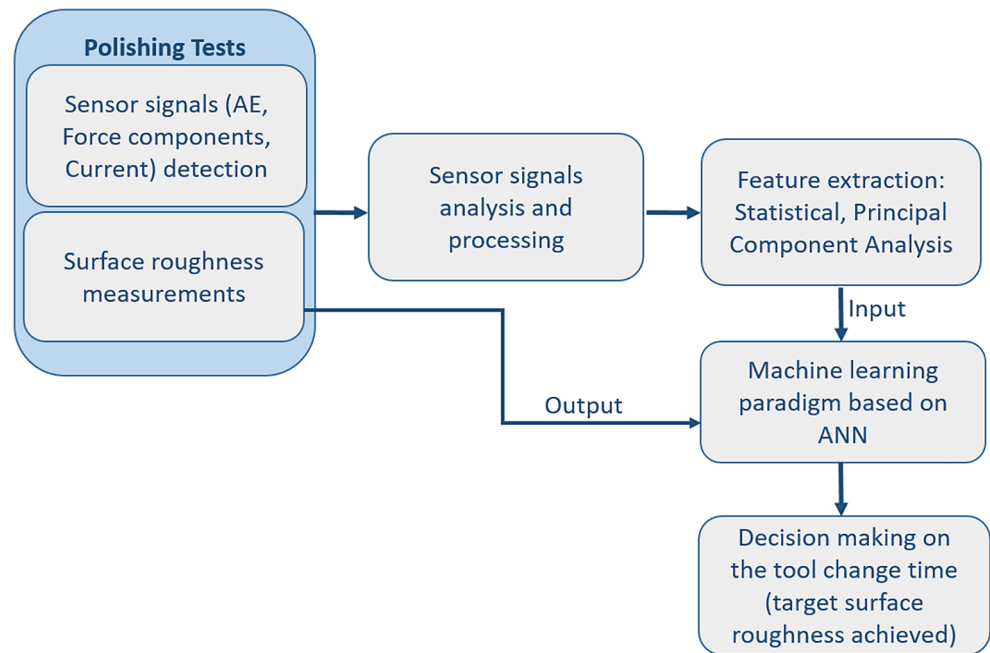
The application of sensor monitoring for the detection of abrasive process state was demonstrated in several research works. Chang et al. [5] utilized an acoustic emission setup for in-process material removal monitoring in lapping. In [6], a process-machine interaction model using a multi-sensor fusion approach was proposed and experimentally tested to predict surface roughness in cylindrical plunge grinding. In [7],

✉ Tiziana Segreto
tsegreto@unina.it

¹ Fraunhofer Joint Laboratory of Excellence on Advanced Production Technology (Fh-J_LEAPT UniNaples), Naples, Italy

² Department of Chemical, Materials and Industrial Production Engineering, University of Naples Federico II, P.le Tecchio 80, 80125 Naples, Italy

Fig. 1 Scheme of the in-process surface roughness prediction



methods for in-process sensor monitoring of jet conditions in abrasive waterjet machining were tested, discussed, and classified. The types of sensors for process monitoring in abrasive processes were extensively discussed in [8]. As regards robot-assisted finishing, Dieste et al. [9] investigated the parameters influencing grinding and polishing processes in order to develop an automatic system based on a spherical robot.

Despite the numerous scientific papers on abrasive process monitoring, studies on the improvement of polishing

technologies using multiple sensors are quite few. An intelligent polishing system using acoustic emission sensors to improve the surface quality of sculptured die surfaces on a five-axis polishing machine was proposed by [10]. Pilný and Bissacco [11] developed a monitoring and control strategy for automatic detection of process end point in robot-assisted polishing. In [12], a computer-based monitoring of polishing processes was developed in the LabView environment for online calculation of mechanical, chemical, and thermal indicators, allowing for the analysis of the polishing behavior of various work materials.

The main goal of this paper is the detection of the right time for tool change, defined as end-point detection (EPD), in robot-assisted polishing (RAP) in order to obtain the desired finished part characteristics and quality, including the

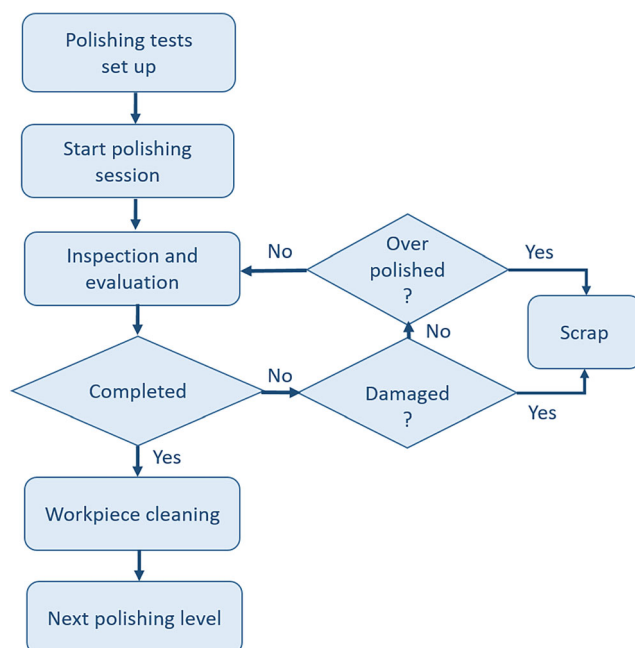


Fig. 2 Polishing phases

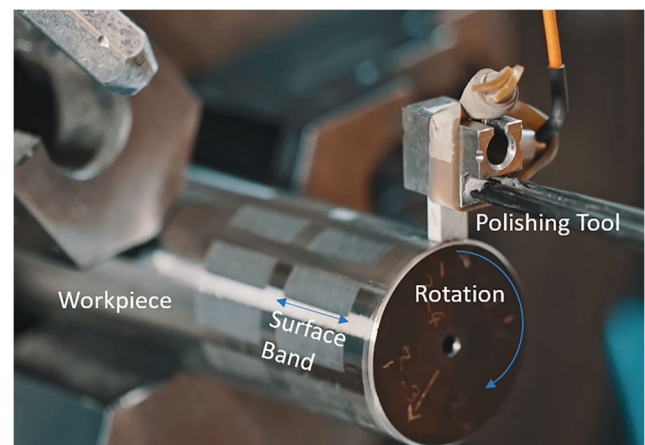


Fig. 3 Experimental polishing test

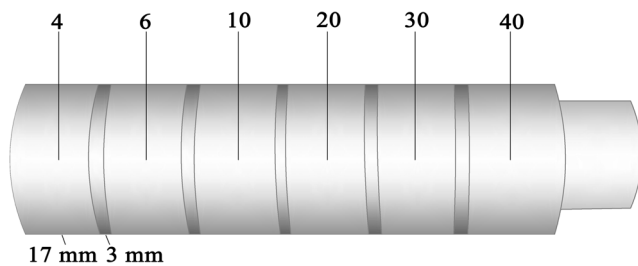


Fig. 4 Cylindrical workpiece with six surface bands of 17 mm width, separated by 3 mm spacing: each band was subjected to 4, 6, 10, 20, 30, or 40 polishing passes

achievement of the target surface roughness level. A multiple-sensor monitoring approach for polishing process control can be a solution for EPD allowing for automatic process termination and/or tool change, with significant reduction of the polishing cycle time while complying with the specified geometrical tolerances by avoiding excessive material removal.

In this work, a multiple sensor monitoring system comprising three different sensing units (acoustic emission, strain and current sensors) was set up and utilized to collect in-process data in order to determine the polishing process state and the achievement of the target surface roughness by making use of sensor fusion technology merging information from sensor signals of different nature [13, 14] and machining learning paradigms based on artificial neural networks (ANNs) [15, 16]. During the experimental polishing tests, surface roughness measurements were carried out on the polished surfaces after different numbers of polishing passes. The detected signals were pre-processed and analyzed by applying two types of feature extraction procedures: statistical feature extraction and principal component analysis (PCA). PCA is an advanced feature extraction methodology that allows to reduce the dimensionality of sensorial features, thus lowering the number of data sets. The selected principal components and the calculated statistical features were utilized to develop machine learning paradigms, based on ANNs, for surface roughness assessment in order to predict the end point of the polishing process when the target surface roughness is achieved.

In-process surface roughness prediction has the following advantages (Fig. 1):

- It indicates if and when the target surface roughness is reached in the polishing process.
- In case the surface roughness evolution deviates from the reference trend, the process can either be shortened or prolonged till the target surface roughness is achieved.

Table 1 Polishing tests

Surface band	1	2	3	4	5	6
No. of passes	4	6	10	20	30	40

- Even if the target surface roughness is not achievable for some reason, it still signals the right time to change the tool in order to avoid the occurrence of over-polishing.

2 Materials and methods

The polishing process investigated in this paper is carried out using a RAP machine where a motorized arm is utilized in substitution of the human operator. Generally, the phases of a polishing operation are the following (Fig. 2):

1. Setting up the machine and the tool and clamping the workpiece. Moreover, the main polishing parameters are set: spindle rotational speed, cutting speed, cutting force, stroke length, and pulse rate.
2. Executing the polishing sessions. The polishing process is carried out based on the amount of material to be removed to achieve the target surface roughness, the workpiece material type, and the initial surface roughness value.
3. Stopping the polishing process for inspection and evaluation of the workpiece state using measurement devices.
4. Based upon the inspection assessment, either:
 - continue with the current polishing step
 - change to the next polishing step
 - consider the part as finished
 - scrap the part if it is damaged

The polishing process monitoring approach developed in this paper involves the use of multiple sensors, signal processing, sensor fusion, and machine learning paradigms in order to realize a predictive system capable to decide on the next polishing step to be performed, instead of following the traditional method previously described.

2.1 Experimental set-up

The experimental campaign was carried out on four cylindrical bars made of tool steel hardened to 57–58 HRC (Hardness Rockwell C), with \varnothing 40 mm and 100 mm length, finish turned to a surface roughness of approximately $S_a = 0.3 \mu\text{m}$.

A silicon carbide polishing stone with #800 grit size was used as polishing tool with the following parameters: 9 N contact force, 1000 pulses/min oscillation frequency with 1-mm stroke length, 200 rpm workpiece rotational speed, 1 mm/s feed rate (Fig. 3).

The polishing tests were performed in six steps (Fig. 4): for every workpiece, six surface bands, each of 17 mm width, separated by 3 mm spacing, were progressively polished by 4, 6, 10, 20, 30, and 40 passes with unidirectional axial tool travel (Table 1).

Table 2 F_x , F_y , F_z , and Current sensor signal data files for the four workpieces

Workpiece	Column 1-2-3-4-5	# of samplings	Time (min)	Sampling rate (kS/s)
WP1	Time, F_x , F_y , F_z , Current	1,416,000	11.8	2
WP2	Time, F_x , F_y , F_z , Current	1,392,000	11.6	2
WP3	Time, F_x , F_y , F_z , Current	1,408,000	11.7	2
WP4	Time, F_x , F_y , F_z , Current	1,395,000	11.6	2

A polishing pass, defined as the path of the polishing tool to go from one end of the desired length to be polished to the other extremity, had a length of 17 mm equal to the surface bands width. The duration of each polishing session, covering the 40 polishing passes, was approximately 11.6 min (Table 2). As each single pass corresponded to 17 mm and the utilized feed rate was 1 mm/s, one pass required about 17 s to be completed.

2.2 Multiple-sensor monitoring system

The in-process multiple-sensor monitoring system utilized for signal acquisition comprised three different sensing units: an acoustic emission (AE), a strain gage, and a current sensor [17–19].

The AE sensor was mounted on the tool holder, as close as possible to the polishing stone to minimize the signal loss and achieve a good signal-to-noise ratio, and possessing the following characteristics: resonant frequency (kHz): $300 \pm 20\%$, sensitivity dB (0 dB = 1 V/m/s): 115 ± 3 , temperature range (°C): $-20 \sim +80$. The AE signals were pre-amplified and high-pass filtered with a 50 kHz cut-off frequency. The amplified signal output was directly connected, via coaxial cable, to a multifunction data acquisition board with a sampling frequency of 1 MHz and 16-bit resolution. The high sampling frequency of 1 MHz was chosen to ensure suppression of signal aliasing and possible loss of signal amplitude due to any high frequencies present.

The strain gage sensor was located between the tool holder and the robotic arm to detect the three components of the polishing force which were digitized with sampling rate 2 kS/s. The detected force components are: F_x = friction force in the tool oscillation direction, parallel to the workpiece axis; F_y = friction force in the workpiece rotation direction,

tangential to the cylindrical bar; F_z = normal contact force in the radial workpiece direction.

The current sensor was mounted in the electrical cabinet of the RAP machine to detect the current signals, related to the motor power absorbance, which were digitized with sampling rate 2 kS/s.

The sensor signals were digitalized using a DAQ board and were sent to a PC for processing and analysis. The number of samplings for each detected sensor signal file depends on the sampling rate utilized during signal acquisition and is reported in Tables 2 and 3 for the 40 polishing passes of each test. For sensor signals detected with sampling rate 2 kS/s, one polishing pass corresponds to about 34,100 samplings. For AE sensor signals detected with sampling rate 1 MS/s, a total number of 1409 files (WP1 = 446, WP2 = 335, WP3 = 347, WP4 = 281) were obtained, each containing 500,000 samplings (Table 3). The total number of AE files for each workpiece was divided by the number of passes (40 passes) in order to obtain an approximate number of AE files per pass.

2.3 Surface roughness measurements

The main surface quality indicator of a machined workpiece is its surface roughness. Mechanical devices with a stylus probe are widely utilized to measure surface roughness with good accuracy. However, the main disadvantages of these contact systems are represented by low measuring speed and surface damage by the stylus probe, particularly for soft materials [20]. These problems can be overcome by utilizing non-contact methods, usually optical, which allow to measure the height variations on surfaces with high precision using the wavelength of light as the ruler [21, 22].

Generally, surface roughness is evaluated through 2D profilometry parameters such as the roughness average, R_a ,

Table 3 AE sensor signal data files for the four workpieces

Workpiece	From	To	# of samplings	Sampling rate	Number of files/pass
WP1	AE_0001	AE_0446	500,000	1 MHz	11.2
WP2	AE_0001	AE_0335	500,000	1 MHz	8.4
WP3	AE_0001	AE_0347	500,000	1 MHz	8.7
WP4	AE_0001	AE_0281	500,000	1 MHz	7.0

Table 4 Five measurements of areal surface roughness parameter S_a and their average values for each of the six surface bands of each of the four workpieces

Meas. #	S_a [nm] for WP1							S_a [nm] for WP2						
	Ini.	B1	B2	B3	B4	B5	B6	Ini.	B1	B2	B3	B4	B5	B6
1	370	68	83	62	38	41	45	374	129	57	51	48	47	42
2	345	64	67	62	44	45	42	284	75	79	63	49	45	42
3	326	74	63	73	43	41	43	351	77	67	47	49	45	41
4	379	86	121	46	51	40	41	265	96	64	54	80	39	39
5	312	77	109	58	51	47	48	257	85	65	36	42	43	35
Avg.	346	74	88	60	45	43	44	306	92	66	50	54	44	40
Meas. #	S_a [nm] for WP3							S_a [nm] for WP4						
	Ini.	B1	B2	B3	B4	B5	B6	Ini.	B1	B2	B3	B4	B5	B6
1	346	143	91	78	89	63	70	365	108	61	55	50	39	44
2	396	68	105	67	55	59	56	414	89	70	52	51	45	32
3	348	80	75	59	65	73	44	312	96	66	61	61	58	66
4	250	63	70	55	55	47	37	381	74	68	69	40	46	36
5	326	168	50	52	48	49	44	391	82	60	45	34	38	34
Avg.	333	104	78	62	62	58	50	373	90	65	56	47	45	43

defined as the arithmetic average of the absolute values of the profile heights over the evaluation length and given by Eq. (1):

$$R_a = \frac{1}{L} \int_0^L |y(x)| dx \tag{1}$$

where L is the sampling length and y is the coordinate of the profile curve.

In 3D optical profilometry, surface roughness is specified through areal measurements. The ISO 25178 norm specifies the terms, definitions, and parameters to determine the surface texture by areal methods (<https://www.iso.org>). In particular, the surface area roughness parameter, S_a , is defined as the arithmetic mean of the absolute of the ordinate values within a definition area A and given by Eq. (2):

$$S_a = \frac{1}{A} \iint_A |z(x, y)| dx dy \tag{2}$$

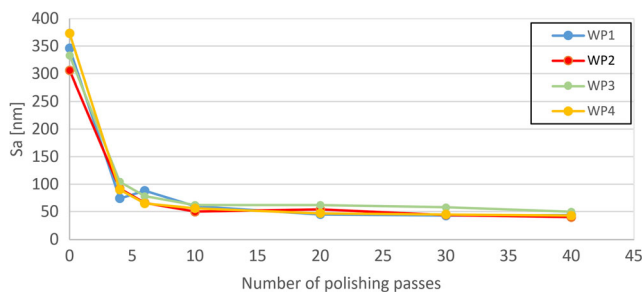


Fig. 5 Average values of the areal surface roughness parameter, S_a , plotted versus the number of polishing passes for the four workpieces WP1, WP2, WP3, and WP4

Moreover, the root mean square roughness parameter, S_q , is mathematically evaluated over the complete 3D surface by EQ. (3):

$$S_q = \sqrt{\iint_a (Z(x, y))^2 dx dy} \tag{3}$$

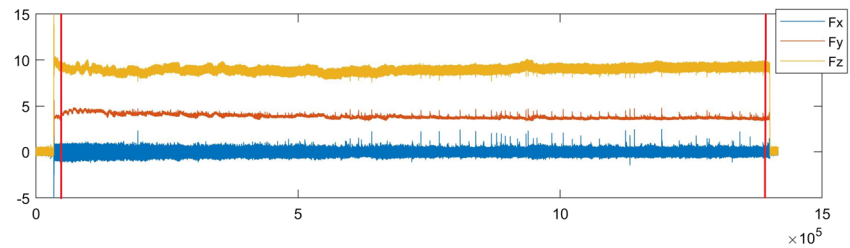
The areal surface roughness parameters S_a and S_q represent an overall measure of the surface texture: S_q is typically used to specify optical surfaces and S_a is mainly utilized for machined surfaces (<https://www.iso.org>).

To specify the polished surface texture, areal surface roughness measurements were carried out on each surface band using a confocal microscope with 50× magnification, a vertical resolution of 3 nm, and a measurement time > 3 s. The selected areal surface roughness parameter was S_a as the workpieces under investigation are not characterized by optical surfaces but by machine-polished surfaces. The measurements were performed off-line before and after polishing on five random locations on each surface band. In Table 4, the five measured S_a values and their average are reported for the

Table 5 Number of samplings for each segmentation step

Workpiece	# of samples for the raw F_x, F_y, F_z and Current sensor signals	# of samples for the truncated (head and tail) F_x, F_y, F_z and Current sensor signals	# of samples for each polishing pass
WP1	1,416,000	1,364,000	34,100
WP2	1,392,000	1,363,379	34,084
WP3	1,408,000	1,366,639	34,166
WP4	1,395,000	1,365,499	34,137

Fig. 6 F_x , F_y , F_z and Current sensor signal segmentation for WP1 (40 passes)



four workpieces WP1, WP2, WP3, and WP4. In Fig. 5, the average values of areal surface roughness parameter S_a are plotted versus the number of polishing passes for each of the four workpieces. The figure shows that the trend of the four curves displays a high decrease of average surface roughness during the first ten passes of the polishing process for all four workpieces. Further polishing passes provide only minor improvements of the polished surface. Therefore, the completion of the first ten polishing passes can represent the right time to terminate the polishing process.

3 Sensor signal processing and analysis

3.1 Signal pre-processing

The acquired sensor signals (F_x , F_y , F_z , Current, and AE) were subjected to a pre-processing phase consisting of sensor signal conditioning and segmentation.

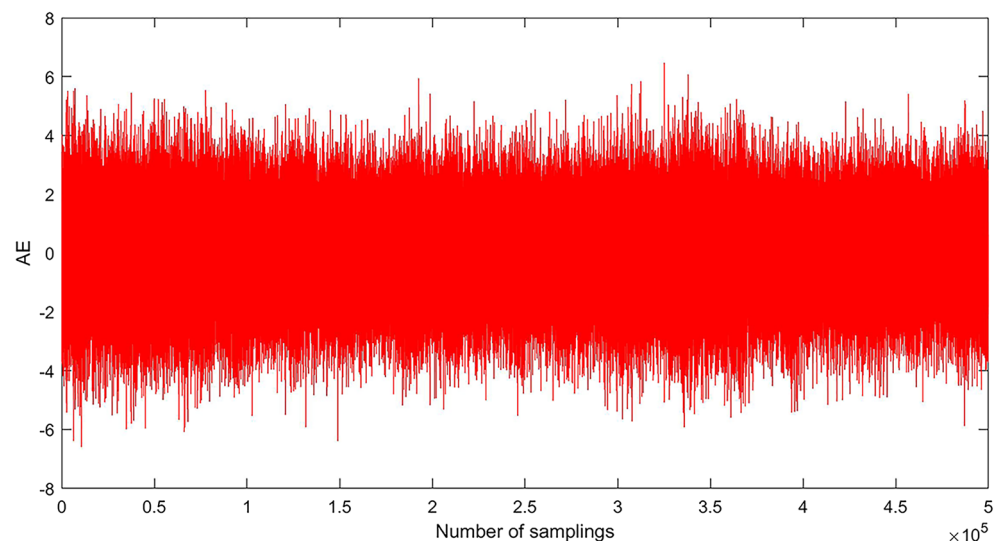
A first segmentation of the F_x , F_y , F_z , and Current sensor signals was carried out to remove the transient conditions not related to the regime polishing process: the head and tail of the sensor signals, which correspond to the beginning and the end of the polishing process, were removed. Then, the segmented F_x , F_y , F_z , and Current signals were subdivided into 40

portions to obtain the number of signal samplings corresponding to each single pass (Table 5). In Fig. 6, the red vertical lines represent the cut off of the head and the tail of the F_x , F_y , F_z , and Current signals for workpiece WP1 (40 passes).

As regards the AE signals, the utilized AE sensor generated an electrical offset which made the AE signals oscillate around a non-zero value representing a signal bias that had to be removed. Thus, a signal shifting procedure was applied: the signal mean value was calculated and subtracted from each complete signal to obtain a typical AE raw signal oscillating around zero. In Fig. 7, an example of shifted AE signal, comprising 500,000 samplings, is reported for WP3.

Then, the AE shifted signals were subjected to the same signal segmentation procedure applied to the force and current signals in order to remove the transient phases of the polishing process. The number of AE files for each polishing pass depends on the polishing tests (Table 3). In particular, for WP1 the number of files for each polishing pass is equal to 11.2, for WP2 is 8.4 files/pass, for WP3 is 8.7 files/pass, and for WP4 is 7.0 files/pass. Therefore, for each workpiece, a group of AE sensor signal files ranging from 7 (WP4) to 11 (WP1) was obtained. Only the central portion of these groups, corresponding to three equal subgroups of 500,000 samplings, was considered for features extraction to avoid too large AE data size while keeping the core data.

Fig. 7 Shifted AE sensor signal for WP3 (40 passes)



3.2 Signal feature extraction procedures

Diverse techniques are available for feature extraction from sensorial data [23]. The main advantage of these methodologies is the size reduction of sensorial data input to knowledge-based models [24] allowing for less complex learning paradigms based on small and robust datasets [25].

In this paper, two feature extraction methods were applied to the pre-processed sensor signals: (a) principal component analysis and (b) statistical feature extraction. The extracted features were employed to construct different feature pattern vectors, including the application of sensor fusion technology.

3.2.1 Principal component analysis for feature extraction and pattern vector construction

The advances in information and communication technologies, embedded computers and networks, and sensorial physical systems allow for the detection and storage of “big data” obtained from measurements carried out on manufacturing processes. These measured data are a rich source of information which, when usefully exploited, can greatly enhance the manufacturing process performance. The knowledge embedded in the data can be effectively extracted to construct accurate models able to describe, summarize, and predict the process behavior [26].

Principal component analysis (PCA) is an advanced multivariate data analysis technique utilized to extract information from data by relating its variables. It transforms interrelated variables by rotating their axes of representation retaining as much as possible of the variation of the original variables in a lower dimension space. The new axes of rotation are represented by the projection directions or principal component loadings. The obtained principal components (PCs) are uncorrelated and ordered so that the first few retain most of the variance present in all of the original variables [27–30].

The PCA procedure implemented in this paper was applied to the five statistical feature vectors extracted in Section 3.2 in order to find the principal components for each F_x , F_y , F_z , Current, and AE sensor signals for each of the four workpieces WP1, WP2, WP3, and WP4.

The PCA algorithm receives as input an $n \times j$ matrix, where n is the number of the polishing passes, equal to 40, and j is the number of statistical features, equal to 5 (40×5 matrix). The PCA returns the principal component scores (a representation of the data matrix in the principal component space) where the rows correspond to the observations and the columns correspond to the components; a vector (latent) containing the eigenvalues of the covariance matrix of the input matrix; a $j \times j$ matrix where each column contains the coefficients for one principal component. Five principal components, PC₁, PC₂, PC₃, PC₄, and PC₅, were generated. The criterion for selecting the number of suitable principal components is based on the

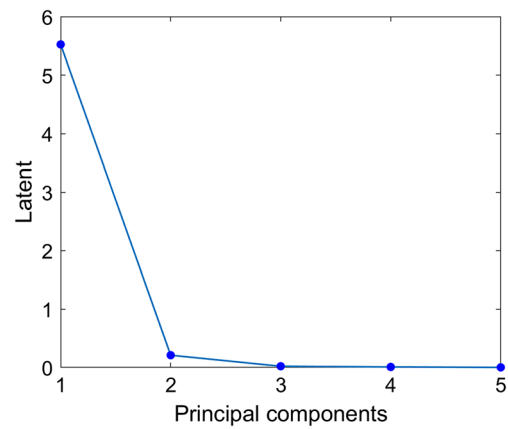


Fig. 8 Scree plot of the eigenvalues for the F_x force component in the case of WP1

evaluation of the covariance matrix or “latent roots” [31, 32]. The latter represent the amount of variance explained by each principal component; they are required to decrease monotonically from the first to the last principal component and are represented by a scree plot. A scree plot is a simple line segment plot that shows the fraction of total variance in the data as explained or represented by each principal component. Such a plot, when read from left to right across the abscissa, can often show a clear separation in the fraction of total variance where the “most important” components cease and the “least important” ones begin. The point of separation is often called the “elbow”. In the PCA literature, the plot is called a “scree” plot because it often looks like a “scree” slope where rocks have fallen down and accumulated on the side of a mountain [31, 32].

Figure 8 shows the scree plot reporting the variance explained versus the principal components for the F_x force component in the case of WP1. It can be observed that the elbow occurs between the 2nd and 3rd principal components indicating that two components are sufficient to describe the variance of the data.

A visual analysis of each generated scree plot was performed showing the same behavior of Fig. 8. Therefore, the two obtained principal components (PC₁, PC₂: energy and mean, respectively), in terms of score matrix, for each sensor signal (F_x , F_y , F_z , Current, AE) and each workpiece (WP1,

Table 6 Extracted statistical features

	F_x	F_y	F_z	AE	Current
Mean	F_{xMean}	F_{yMean}	F_{zMean}	AE_{Mean}	Cur_{Mean}
Variance	F_{xVar}	F_{yVar}	F_{zVar}	AE_{Var}	Cur_{Var}
Skewness	F_{xSke}	F_{ySke}	F_{zSke}	AE_{Ske}	Cur_{Ske}
Kurtosis	F_{xKur}	F_{yKur}	F_{zKur}	AE_{Kur}	Cur_{Kur}
Energy	F_{xEn}	F_{yEn}	F_{zEn}	AE_{En}	Cur_{En}

Table 7 PCA feature input pattern vectors and ANN configurations

PCA feature input pattern vector	ANNs configurations		
Two-element consisting of the two principal components for each sensor signal F_x, F_y, F_z , Current, and AE	2-2-1	2-4-1	2-8-1
Six-element combining the two principal components calculated for the F_x, F_y , and F_z sensor signals	6-6-1	6-12-1	6-18-1
Eight-element combining the two principal components obtained for the F_x, F_y, F_z and Current signals	8-8-1	8-16-1	8-24-1
Ten-element combining the two principal components for all the sensor signals	10-10-1	10-20-1	10-30-1

WP2, WP3, WP4) were used to construct diverse PCA feature pattern vectors for machine learning paradigm development:

- Two-element PCA feature pattern vector composed of the two principal components for each sensor signal F_x, F_y, F_z , Current, and AE. For example, in the case of F_x , the 2-element PCA feature pattern vector is: [1st PCA_{F_x} , 2nd PCA_{F_x}].
- Six-element PCA feature pattern vector consisting of the two principal components calculated for the F_x, F_y , and F_z sensor signals: [1st PCA_{F_x} , 2nd PCA_{F_x} , 1st PCA_{F_y} , 2nd PCA_{F_y} , 1st PCA_{F_z} , 2nd PCA_{F_z}].
- Eight-element PCA feature pattern vector consisting of the two principal components obtained for the F_x, F_y, F_z and Current signals: [1st PCA_{F_x} , 2nd PCA_{F_x} , 1st PCA_{F_y} , 2nd PCA_{F_y} , 1st PCA_{F_z} , 2nd PCA_{F_z} , 1st PCA_{Curr} , 2nd PCA_{Curr}].
- Ten-element PCA feature pattern vector corresponding to the two principal components for all the sensor signals: [1st PCA_{F_x} , 2nd PCA_{F_x} , 1st PCA_{F_y} , 2nd PCA_{F_y} , 1st PCA_{F_z} , 2nd PCA_{F_z} , 1st PCA_{Curr} , 2nd PCA_{Curr} , 1st PCA_{AE} , 2nd PCA_{AE}].

The six-, eight-, and ten-element PCA feature pattern vectors represent sensor fusion feature pattern vectors because they combine the information provided by sensor signals of diverse nature.

3.2.2 Statistical features extraction and pattern vector construction

A statistical feature extraction technique was applied to each F_x, F_y, F_z , Current, and AE signal in the time domain

Table 8 Statistical feature input pattern vectors and ANN configurations

Statistical feature input pattern vector	ANN configurations		
Five-element consisting of the five statistical features for each sensor signal F_x, F_y, F_z , Current, AE	5-5-1	5-10-1	5-15-1
15-element combining the five statistical features extracted from the F_x, F_y, F_z sensor signals	15-15-1	15-30-1	
20-element combining the five statistical features extracted from F_x, F_y, F_z , and Current sensor signals	20-20-1	20-40-1	
25-element combining the five statistical features extracted from all sensor signals	25-25-1	25-50-1	

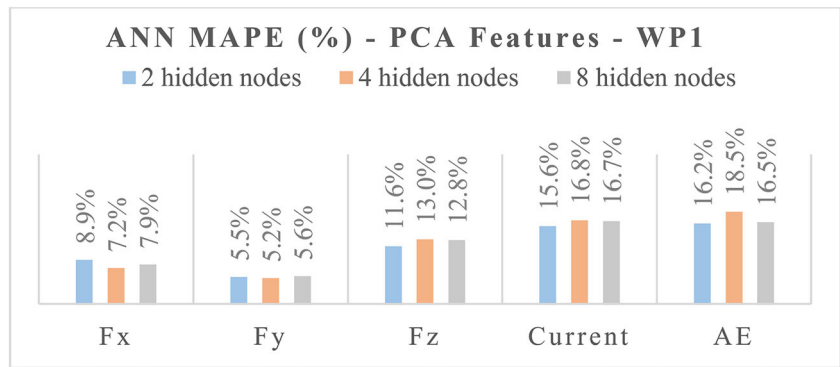
calculating five statistical features: mean, variance, skewness, kurtosis, and energy (Table 6).

With the extracted statistical features, diverse statistical feature pattern vectors were built to be used in machine learning paradigms:

- Five-element statistical feature pattern vector consisting of the five statistical features extracted for each sensor signal. For example, in the case of F_x , the five-element statistical feature pattern vector was: [$F_{xMean}, F_{xVar}, F_{xSke}, F_{xKur}, F_{xEn}$].
- 15-element statistical feature pattern vector combining the five statistical features extracted from the three force component signals F_x, F_y, F_z : [$F_{xMean}, F_{xVar}, F_{xSke}, F_{xKur}, F_{xEn}, F_{yMean}, F_{yVar}, F_{ySke}, F_{yKur}, F_{yEn}, F_{zMean}, F_{zVar}, F_{zSke}, F_{zKur}, F_{zEn}$].
- 20-element statistical feature pattern vector combining the five statistical features extracted from F_x, F_y, F_z , and Current signals: [$F_{xMean}, F_{xVar}, F_{xSke}, F_{xKur}, F_{xEn}, F_{yMean}, F_{yVar}, F_{ySke}, F_{yKur}, F_{yEn}, F_{zMean}, F_{zVar}, F_{zSke}, F_{zKur}, F_{zEn}, Cur_{Mean}, Cur_{Var}, Cur_{Ske}, Cur_{Kur}, Cur_{En}$].
- 25-element statistical feature pattern vector combining the five statistical features extracted from all sensor signals: [$F_{xMean}, F_{xVar}, F_{xSke}, F_{xKur}, F_{xEn}, F_{yMean}, F_{yVar}, F_{ySke}, F_{yKur}, F_{yEn}, F_{zMean}, F_{zVar}, F_{zSke}, F_{zKur}, F_{zEn}, Cur_{Mean}, Cur_{Var}, Cur_{Ske}, Cur_{Kur}, Cur_{En}, AE_{Mean}, AE_{Var}, AE_{Ske}, AE_{Kur}, AE_{En}$].

The 15-, 20-, and 25-element statistical feature pattern vectors represent sensor fusion feature pattern vectors because they combine the information provided by sensor signals of different nature.

Fig. 9 ANN MAPE results for the two-element PCA feature pattern vector for each sensor signal F_x, F_y, F_z , Current, AE, and for each ANN configuration in the case of the WP1



4 Machine learning based on artificial neural networks for polishing end-point prediction

Machine learning paradigms based on artificial neural networks (ANNs) [15, 16] were employed for surface roughness assessment in order to obtain the end-point prediction (EPD) of the polishing process. The intelligent prediction of surface roughness allows to make a decision on the appropriate stopping time during the polishing process so as to avoid over-polishing and the consequent potential defects in the workpiece. ANNs are intelligent computing systems trained to perform specific functions. In particular, they are employed for pattern recognition–based decision making for mapping procedures through which points in the input space are associated with corresponding points in the output space on the basis of designated attribute values, of which class membership can be one [33].

In this paper, three-layer cascade-forward backpropagation ANNs were built with diverse configurations using as input either the obtained PCA feature pattern vectors or the calculated statistical feature pattern vectors and as output the surface roughness level for each polishing pass obtained by interpolating the average areal surface roughness values reported in Section 2.3 for every workpiece. A growing number of hidden layer nodes was selected in order to find the ANNs configuration with the highest performance. As a matter of fact, the most common approach to find the optimal size of a

ANN configuration is to try different architecture with different hidden nodes [16, 34]. For ANNs training, a Levenberg-Marquardt optimization algorithm [33] was chosen as training function and the mean square error was used as objective function, while the tan-sigmoid was selected as transfer function. The number of epochs was set equal to 1000 and the minimum performance gradient was set to 1×10^{-7} . The ANNs testing was performed through the leave-k-out method with $k = 1$ [35]: one homogeneous group of k patterns, extracted from the full training set, was held back in turn for testing and the rest of the patterns was used for training.

4.1 ANNs using PCA feature pattern vectors

In the case of the PCA feature pattern vectors, the three-layer feed-forward back-propagation ANNs had the following architecture (Table 7):

- Two-, six-, eight-, or ten-element PCA feature pattern vectors were utilized at input layer
- the number of hidden layer nodes varied between two and 30 depending on the number of input layer nodes;
- the output layer had only one node

Each ANNs training set consisted of 40 input feature pattern vectors, i.e., one input feature pattern vector per polishing

Fig. 10 ANN MAPE results for the two-element PCA feature pattern vector for each sensor signal F_x, F_y, F_z , Current, AE, and for each ANN configuration in the case of WP2

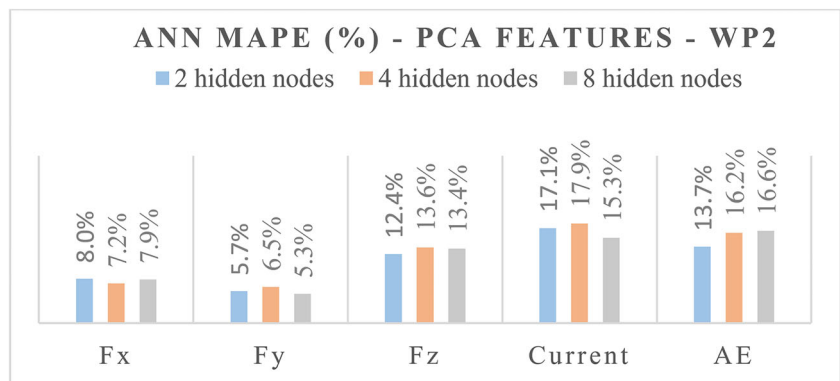
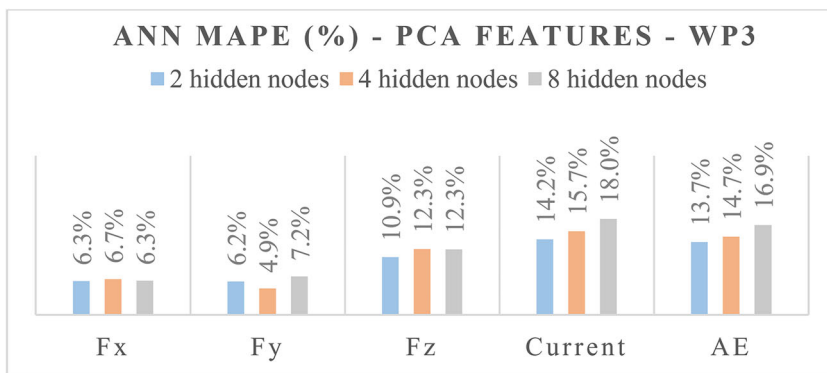


Fig. 11 ANN MAPE results for the two-element PCA feature pattern vector for each sensor signal F_x , F_y , F_z , Current, AE, and for each ANN configuration in the case of WP3



pass, and each of these input feature pattern vectors was associated with the interpolated value of the average areal surface roughness for the corresponding polishing pass. According to the leave-k-out method, at each step, one feature pattern vector was removed in turn from the original training set of 40 feature pattern vectors in order to be used for ANNs testing, while the remaining 39 feature pattern vectors were used for training. This procedure was repeated for all the 40 feature pattern vectors in the training set.

4.2 ANNs using statistical feature pattern vectors

The five-, 15-, 20-, and 25-element statistical feature pattern vectors, constructed with the five statistical features extracted from each sensor signal for every workpiece (Section 3.2.2) were inputted to the ANNs with the configurations summarized in Table 8. The ANNs type, training, and testing had the same characteristics employed for the PCA input feature pattern vectors.

Fig. 12 ANN MAPE results for the two-element PCA feature pattern vector for each sensor signal F_x , F_y , F_z , Current, AE, and for each ANN configurations in the case of WP4

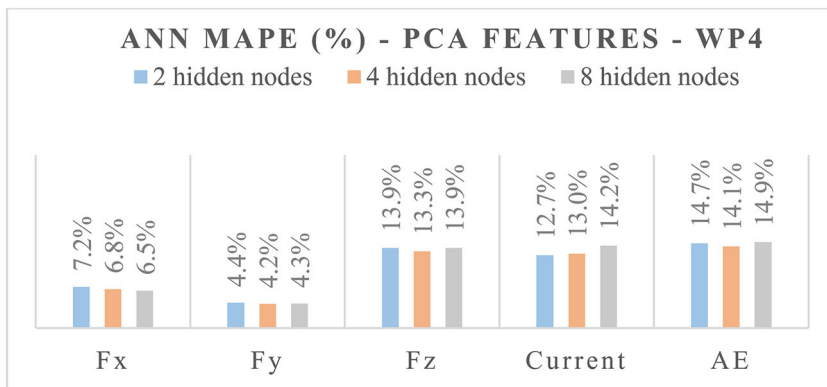


Fig. 13 ANN MAPE results for the six-element PCA feature pattern vector [1st PCA_{F_x} , 2nd PCA_{F_x} , 1st PCA_{F_y} , 2nd PCA_{F_y} , 1st PCA_{F_z} , 2nd PCA_{F_z}] for each ANN configuration and each workpiece

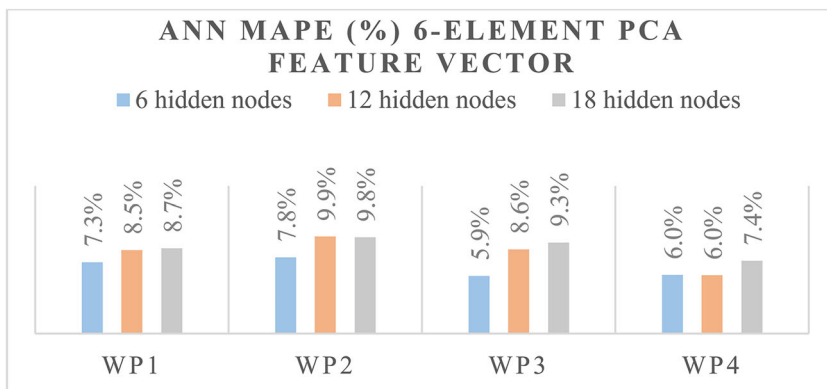
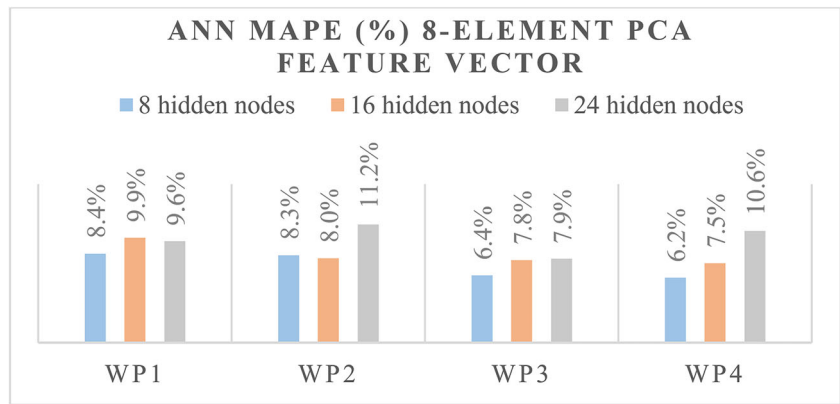


Fig. 14 ANN MAPE results for the eight-element PCA feature pattern vector [1st PCA_{F_x}, 2nd PCA_{F_x}, 1st PCA_{F_y}, 2nd PCA_{F_y}, 1st PCA_{F_z}, 2nd PCA_{F_z}, 1st PCA_{Current}, 2nd PCA_{Current}] for each ANN configuration and each workpiece



5 ANNs results and discussion

The performance of the trained and tested ANNs was estimated in terms of mean absolute percentage error (MAPE), i.e., the absolute differences between target surface roughness values (y_t) and ANNs predicted values (\hat{y}_t) divided by the actual value:

$$MAPE = \frac{100\%}{n} \sum_{t=1}^n \left| \frac{y_t - \hat{y}_t}{y_t} \right|$$

Fig. 15 ANN MAPE results for the ten-element PCA feature pattern vector [1st PCA_{F_x}, 2nd PCA_{F_x}, 1st PCA_{F_y}, 2nd PCA_{F_y}, 1st PCA_{F_z}, 2nd PCA_{F_z}, 1st PCA_{Current}, 2nd PCA_{Current}, 1st PCA_{AE}, 2nd PCA_{AE}] for each ANN configuration and each workpiece

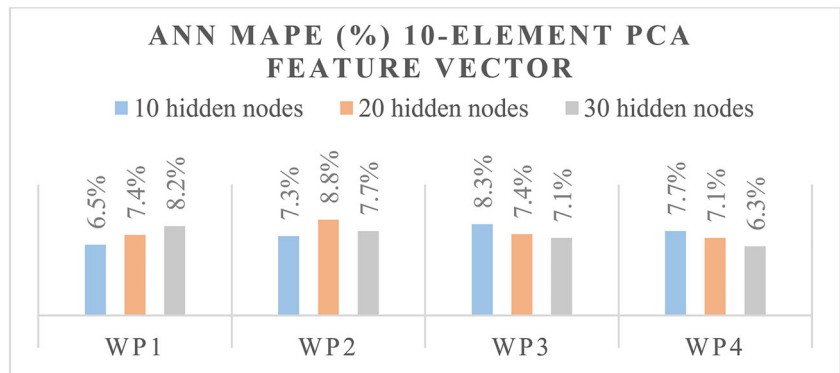
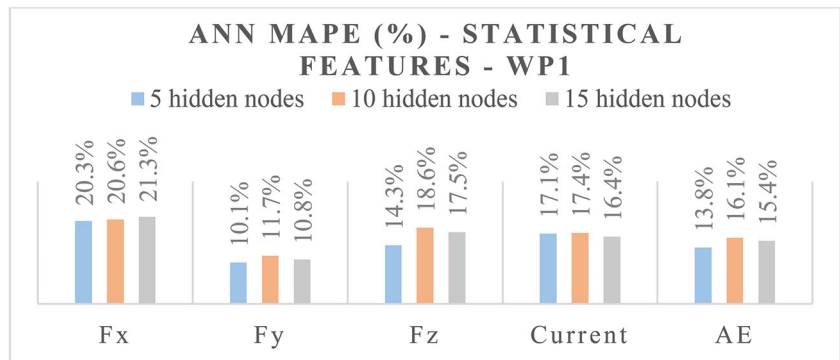


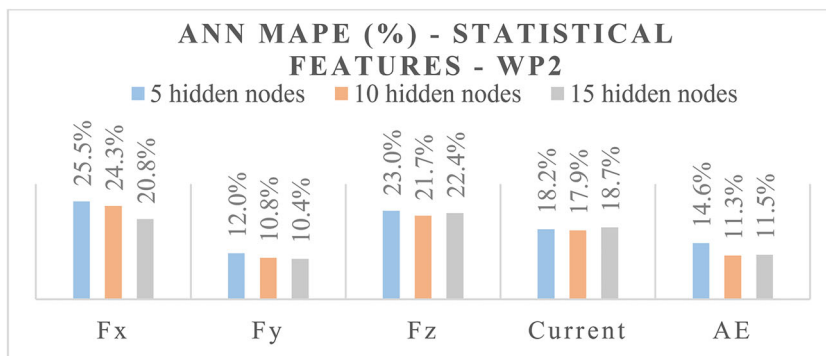
Fig. 16 ANN MAPE results for the five-element statistical feature pattern vectors for each sensor signal F_x , F_y , F_z , Current, AE, and for each ANN configuration in the case of workpiece WP1



5.1 ANNs MAPE results for the PCA feature pattern vectors

In Figs. 9, 10, 11, 12, the ANNs MAPE results (%) are reported for the two-element PCA feature pattern vectors for each sensor signal (F_x , F_y , F_z , Current, AE) and each ANN configuration in the case of workpiece WP1 (Fig. 9), WP2 (Fig. 10), WP3 (Fig. 11), and WP4 (Fig. 12). Figures 13, 14, 15 show the ANNs MAPE results (%) for each workpiece and each ANN configuration for the six-, eight, and ten-element PCA feature pattern vectors.

Fig. 17 ANN MAPE results for the five-element statistical feature pattern vectors for each sensor signal F_x , F_y , F_z , Current, AE, and for each ANN configuration in the case of workpiece WP2



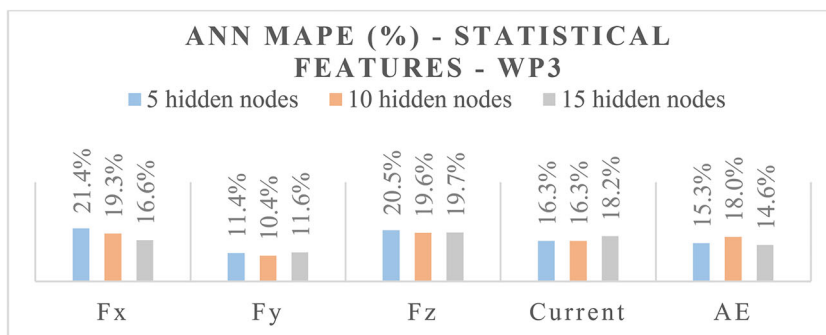
From Figs. 9, 10, 11, 12, 13, 14, 15, a consideration concerning the number of ANNs hidden nodes can be made. From the results of all the ANN configurations for all evaluated cases, it can be seen that increasing the number of hidden nodes does not lead to a meaningful improvement in surface roughness level assessment. This means that the smaller number of hidden nodes allows to effectively find the correlations between input sensorial feature pattern vectors and output surface roughness level, thus allowing to reduce the computational effort and lower the processing time to determine the EPD of the polishing process.

As regards the two-element vectors (Figs. 9, 10, 11, 12), it can be noticed that F_x and F_y present very low ANNs MAPE values, ranging from 6.3 to 8.9% (F_x) and from 4.2 to 7.2% (F_y), displaying a performance in surface roughness assessment for polishing EPD higher than 91.00%. Moreover, F_z , Current, and AE provided interesting MAPE values ranging from 10.9 to 13.9% (F_z), from 12.9 to 18.0% (Current), and from 13.7 to 18.5% (AE), leading to a global ANNs performance in surface roughness assessment for polishing EPD higher than 81.00%.

As regards the sensor fusion PCA feature pattern vectors, it can be noticed that:

- The six-element PCA feature pattern vector provided a very favorable assessment of surface roughness level with an average ANN MAPE value equal to 7.9%, corresponding to an average performance of 92% in surface roughness level assessment for polishing EPD (Fig. 13)

Fig. 18 ANN MAPE results for the five-element statistical feature pattern vectors for each sensor signal F_x , F_y , F_z , Current, AE, and for each ANN configuration in the case of workpiece WP3



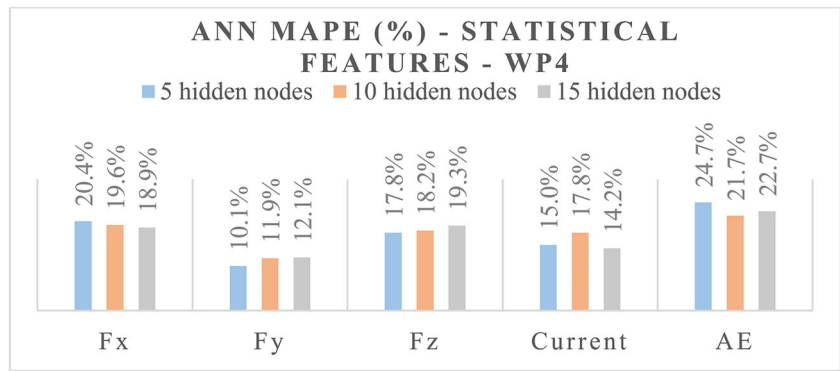
- The eight-element PCA feature pattern vector yielded a good average ANNs MAPE value equal to 8.5% corresponding to an average performance of 91.5% in surface roughness level assessment for polishing EPD (Fig. 14)
- The ten-element PCA feature pattern vector presented the best ANNs MAPE average value (7.5%) corresponding to the highest average performance (92.5%) in surface roughness level assessment for EPD of the polishing process (Fig. 15)

5.2 ANNs MAPE results for the statistical feature pattern vectors

In Figs. 16, 17, 18, 19, 20, 21, 22, the ANNs results, in terms of MAPE (%), are reported for each workpiece and each ANN configuration for the diverse constructed statistical feature pattern vectors. In particular, Figs. 16, 17, 18, 19 report the ANN MAPE results for the five-element statistical feature pattern vectors for each sensor signal and each ANN configuration in the case of workpiece WP1 (Fig. 16), WP2 (Fig. 17), WP3 (Fig. 18), and WP4 (Fig. 19). Figures 20, 21, 22 show the ANN MAPE results for each workpiece and each ANN configuration for the 15-, 20-, and 25-element statistical feature pattern vectors.

Also, in the case of the statistical feature pattern vectors, it can be seen that increasing the number of hidden nodes does not generate a meaningful advantage in the classification of surface roughness level for polishing EPD. From Figs. 16, 17, 18, 19, 20, 21, 22, the following considerations can be made:

Fig. 19 ANN MAPE results for the five-element statistical feature pattern vectors for each sensor signal F_x, F_y, F_z , Current, AE, and for each ANN configuration in the case of workpiece WP4



- In the case of the five-element statistical feature pattern vectors (Figs. 16, 17, 18, 19), the average ANNs MAPE values calculated considering all four workpiece is equal to 20.7% for force component F_x ; 11.1% for force component F_y ; 19.4% for force component F_z ; 17.0% for Current; and 16.7% for AE. These results highlight that the force component F_y provided the best ANNs classification of surface roughness level for polishing EDP.

As regards the sensor fusion statistical feature pattern vectors, it can be noticed that:

- The 15-element statistical feature pattern vector, obtained by combining the five statistical features extracted from the F_x, F_y, F_z signals, presented a minimum and maximum ANN MAPE value equal to 13.2% and 18.8%, respectively (Fig. 20)
- The 20-element statistical feature pattern vector, obtained by combining the five statistical features extracted from the F_x, F_y, F_z , and Current signals, showed a minimum and maximum ANN MAPE value equal to 10.4% and 18.4%, respectively (Fig. 21)
- The 25-element statistical feature pattern vector, obtained by combining the five statistical features extracted from all sensor signals, the minimum and maximum ANN MAPE values are equal to 9.9% and 16.4%, respectively (Fig. 22)

Thus, the 25-element sensor fusion statistical feature pattern vector presented the lowest ANN MAPE values, corresponding to an average ANN MAPE of 86.8%, providing the most effective assessment of surface roughness level for EPD of the polishing process.

5.3 Comparison

By comparing the number of ANNs input layer nodes for the PCA and the statistical feature extraction procedures, in the case of PCA feature pattern vectors, the number of input nodes (2, 6, 8, and 10) was always smaller than for statistical feature pattern vectors (5, 15, 20, and 25). This entails a lower computational effort and consequent shorter data processing time.

By comparing the ANN MAPE results, it can be noticed that:

- The ANN MAPE values obtained for PCA feature pattern vectors are lower than those obtained for statistical feature pattern vectors.
- The two-element PCA feature pattern vectors have a similar behavior as the five-element statistical feature pattern vectors, highlighting that the F_y force component provides the best ANN MAPE results. In the case of the PCA feature pattern vector, the F_y force component provides the best overall ANN MAPE results (4.2%).

Fig. 20 ANN MAPE results for the 15-element statistical feature pattern vector: [$F_{xMean}, F_{xVar}, F_{xSke}, F_{xKur}, F_{xEn}, F_{yMean}, F_{yVar}, F_{ySke}, F_{yKur}, F_{yEn}, F_{zMean}, F_{zVar}, F_{zSke}, F_{zKur}, F_{zEn}$] for each ANN configuration and each workpiece

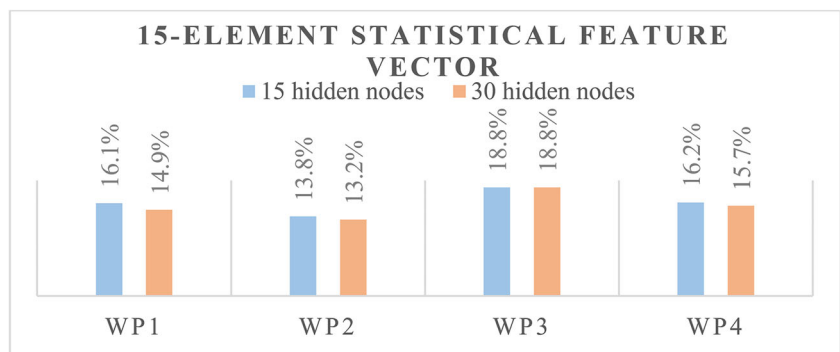
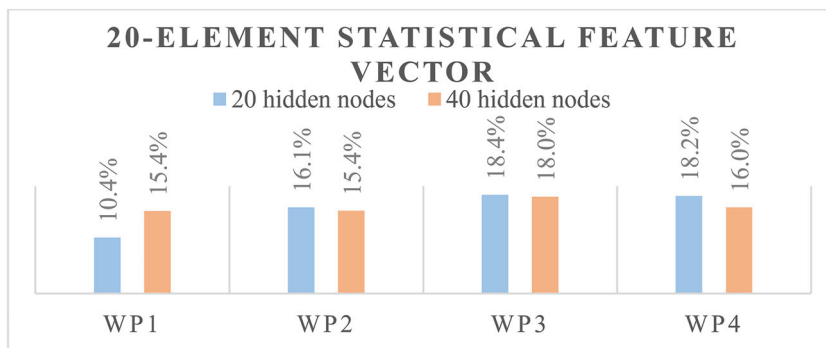


Fig. 21 ANN MAPE results for the 20-element statistical feature pattern vector: $[F_{xMean}, F_{xVar}, F_{xSke}, F_{xKur}, F_{xEn}, F_{yMean}, F_{yVar}, F_{ySke}, F_{yKur}, F_{yEn}, F_{zMean}, F_{zVar}, F_{zSke}, F_{zKur}, F_{zEn}, Cur_{Mean}, Cur_{Var}, Cur_{Ske}, Cur_{Kur}, Cur_{En}]$ for each ANN configuration and each workpiece



- The sensor fusion input feature pattern vectors displayed lower ANN MAPE values for both PCA and statistical feature pattern vector cases. In particular, the ten-element PCA feature pattern vector had an ANN MAPE value equal to 7.5% corresponding to a performance as high as 92.5% in surface roughness level assessment for polishing EPD. This confirms the high efficacy of sensor fusion technology in making full use of sensorial information coming from signals of different nature.

6 Conclusions

A multi-sensor monitoring system, comprising an acoustic emission, a strain gage, and a current sensor, was mounted on a RAP machine to determine the right moment for polishing tool change, defined as EPD, in order to obtain the desired surface roughness level in the workpiece. During the experimental tests, multiple sensor signals, F_x , F_y , F_z , Current, and AE, were detected and surface roughness measurements (S_a) were carried out on five generated surface bands of each tested workpiece. The digitized sensor signals were pre-processed and analyzed. Two types of feature extraction procedures were applied: statistical feature evaluation and PCA. The latter is an advanced feature extraction method that allows to reduce the dimensionality of sensorial features by lowering the number of data sets. In this work, two principal components obtained from

PCA were proved to be sufficient to describe the variance of the data.

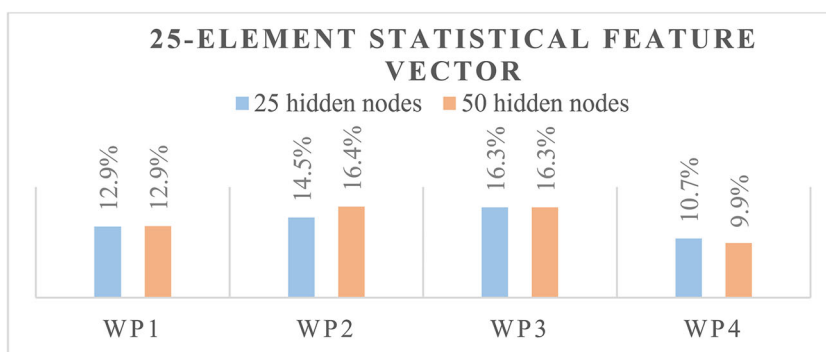
The extracted statistical and PCA features were utilized to construct diverse types of feature pattern vectors to be fed to machine learning paradigms based on ANNs for surface roughness assessment to be utilized for EPD of the polishing process when the target surface roughness is achieved.

In particular, five-, 15-, 20-, and 25-element statistical feature pattern vectors were constructed, and two-, six-, eight-, and ten-element PCA feature pattern vectors were built with the two most relevant principal components (PC_1, PC_2).

By feeding diversely configured ANNs with the statistical and the PCA input feature pattern vectors, a very accurate classification of the polishing process state, in terms of surface roughness level achieved, was accomplished using the PCA feature pattern vectors. The predicted ANN surface roughness values were very close to the measured surface roughness values, with the best mean absolute percentage error equal to 4.2% for the two-element PCA feature pattern vector of the F_y force component, and to 7.5% in the case of the ten-element PCA feature pattern vector.

The proposed approach, involving multiple sensor monitoring, advanced signal processing, and machine learning based on ANNs, was confirmed to be suitable for on-line surface roughness assessment with the aim to determine the appropriate stopping time of polishing processes. This entails the improvement of the RAP machine performance through avoidance of over-polishing and prevention of consequent

Fig. 22 ANN MAPE results for the 25-element statistical feature pattern vector: $[F_{xMean}, F_{xVar}, F_{xSke}, F_{xKur}, F_{xEn}, F_{yMean}, F_{yVar}, F_{ySke}, F_{yKur}, F_{yEn}, F_{zMean}, F_{zVar}, F_{zSke}, F_{zKur}, F_{zEn}, Cur_{Mean}, Cur_{Var}, Cur_{Ske}, Cur_{Kur}, Cur_{En}, AE_{Mean}, AE_{Var}, AE_{Ske}, AE_{Kur}, AE_{En}]$ for each ANN configuration and each workpiece



workpiece defects, thus providing a substantial contribution to the full automation of polishing processes.

Acknowledgments The Fraunhofer Joint Laboratory of Excellence on Advanced Production Technology (Fh-J LEAPT UniNaples) at the Department of Chemical, Materials and Industrial Production Engineering, University of Naples Federico II, is gratefully acknowledged for its support of this research activity.

References

- Evans CJ, Paul E, Dornfeld D, Lucca DA, Byrne G, Tricard M, Klocke F, Dambon O, Mullany BA (2003) Material removal mechanisms in lapping and polishing. *CIRP Ann* 52(2):611–633
- Marinescu I, Uhlmann E, Doi T (2006) *Handbook of lapping and polishing*. CRC Press, Taylor & Francis Group, Boca Raton
- Eriksen RS, Arentoft M, Grønbaek J, Bay N (2012) Manufacture of functional surfaces through combined application of tool manufacturing processes and robot assisted polishing. *CIRP Ann* 61(1):563–566
- Pandiyan V, Tjahjowidodo T (2017) In-process endpoint detection of weld seam removal in robotic abrasive belt grinding process. *Int J Adv Manuf Technol* 93:1699–1714
- Chang YP, Hashimura M, Dornfeld DA (1996) An investigation of the AE signals in the lapping process. *CIRP Ann* 45(1):331–334
- Botcha B, Rajagopal V, Babu NR, Bukkapatnam STS (2018) Process-machine interactions and a multi-sensor fusion approach to predict surface roughness in cylindrical plunge grinding process. *Procedia Manuf* 26:700–711
- Putz M, Dittrich M, Dix M (2016) Process monitoring of abrasive waterjet formation. *Procedia CIRP* 46:43–46
- Inasaki I, Karpuschewski B (2008) Chapter 4.4 - Sensors for process monitoring: abrasive processes, sensors for process monitoring: abrasive processes. In: *Sensors Applications*. Wiley-VCH Verlag GmbH, Weinheim
- Dieste JA, Fernández A, Roba D, Gonzalvo B, Lucas P (2013) Automatic grinding and polishing using spherical robot. *Procedia Eng* 63:938–946
- Ahn JH, Lee MC, Jeong HD, Kim SR, Cho KK (2002) Intelligently automated polishing for high quality surface formation of sculptured die. *J Mater Process Technol* 130:339–344
- Pilný L, Bissacco G (2015) Development of on the machine process monitoring and control strategy in robot assisted polishing. *CIRP Ann* 64(1):313–316
- Klocke F, Dambon O, Schneider U, Zunke R, Waechter D (2009) Computer-based monitoring of the polishing processes using LabView. *J Mater Process Technol* 209:6039–6047
- Mitchell HB (2007) *Multi-sensor data fusion*. Springer-Verlag, Berlin Heidelberg
- Segreto T, Karam S, Simeone A, Teti R (2013) Residual stress assessment in Inconel 718 machining through wavelet sensor signal analysis and sensor fusion pattern recognition. *Procedia CIRP* 9: 103–108
- Bishop CM (2006) *Pattern recognition and machine learning*. Springer-Verlag, New York
- Alpaydin E (2014) *Introduction to machine learning*. MIT Press, Cambridge, MA, USA
- Segreto T, Karam S, Teti R (2017) Signal processing and pattern recognition for surface roughness assessment in multiple sensor monitoring of robot-assisted polishing. *Int J Adv Manuf Technol* 90:1023–1033
- Segreto T, Karam S, Teti R, Ramsing J (2015) Cognitive decision making in multiple sensor monitoring of robot assisted polishing. *Procedia CIRP* 33:333–338
- Segreto T, Karam S, Teti R, Ramsing J (2015) Feature extraction and pattern recognition in acoustic emission monitoring of robot assisted polishing. *Procedia CIRP* 28:22–27
- Bewoor AK, Kulkarni VA (2009) *Metrology & measurement*. McGraw-Hill, New Delhi
- Quinsat Y, Tournier C (2012) In situ non-contact measurements of surface roughness. *Prec Eng* 36:97–103
- Samtaş G (2014) Measurement and evaluation of surface roughness based on optic system using image processing and artificial neural network. *Int J Adv Manuf Technol* 73:353–364
- Teti R, Jemielniak K, O'Donnell G, Dornfeld D (2010) Advanced monitoring of machining operations. *CIRP Ann* 59(2):717–739
- Segreto T (2016) Knowledge-based system. In: *CIRP encyclopedia of production engineering*. Springer Berlin Heidelberg, Berlin, pp 1–5
- Abellan-Nebot JV, Subirón FR (2010) A review of machining monitoring systems based on artificial intelligence process models. *Int J Adv Manuf Technol* 47:237–257
- Nait Malek Y, Kharbouch A, El Khoukhi H, Bakhouya M, De Florio V, El Ouadghiri D, Latre S, Blondia C (2017) On the use of IoT and big data technologies for real-time monitoring and data processing. *Procedia Comput Sci* 113:429–434
- Nounou MN, Bakshi BR, Goel P, Shen X (2002) Bayesian principal component analysis. *J Chemom* 16:576–595
- Jolliffe IT (2002) *Principal component analysis*, 2nd edn. Springer-Verlag New York Inc, New York City
- Segreto T, Simeone A, Teti R (2012) Chip form classification in carbon steel turning through cutting force measurement and principal components analysis. *Procedia CIRP* 2:49–54
- Abdi H, Williams LJ (2010) Principal component analysis. *WIREs Comp Stat* 2:433–459
- Cattell RB (1966) The scree test for the number of factors. *J Multivar Behav Res* 1:245–276
- Segreto T, Simeone A, Teti R (2014) Principal component analysis for feature extraction and NN pattern recognition in sensor monitoring of chip form during turning. *CIRP J Manuf Sci Techy* 7:202–209
- Jordan MI, Bishop CM (2004) *Neural Networks*. In: Tucker AB (ed) *Computer science handbook*, 2nd edn (Section VII: Intelligent Systems). Chapman & Hall/CRC Press LLC, Boca Raton
- Karagiannis S, Stavropoulos P, Ziogas C, Kechagias J (2014) Prediction of surface roughness magnitude in computer numerical controlled end milling processes using neural networks, by considering a set of influence parameters: an aluminium alloy 5083 case study. *Proc IMechE Part B: J Eng Manuf* 228(2):233–244
- Abe S (2001) *Pattern classification: neuro-fuzzy methods and their comparison*. Springer, London, UK

Publisher's note Springer Nature remains neutral with regard to jurisdictional claims in published maps and institutional affiliations.